

## Article

# First Results of Studying EAS Cores Using a High-Mountain Ionization Calorimeter

Turlan Sadykov<sup>1</sup>, Rauf Mukhamedshin<sup>2</sup> , Vladimir Galkin<sup>3</sup> , Alia Argynova<sup>1,\*</sup> , Aidana Almenova<sup>1</sup>, Korlan Argynova<sup>1</sup>, Khanshaiym Makhmet<sup>1,4</sup>, Olga Novolodskaya<sup>1</sup>, Tunyk Idrissova<sup>1</sup> , Valery Zhukov<sup>1,5</sup>, Vyacheslav Piscal<sup>1,5</sup> and Zhakypbek Sadykov<sup>1,6</sup> 

<sup>1</sup> Institute of Physics and Technology, Satbayev University, Almaty 050032, Kazakhstan; turlan43@mail.ru (T.S.); aidana\_alm@mail.ru (A.A.); koraargynova@gmail.com (K.A.); hansh2210@gmail.com (K.M.); novololga@yandex.ru (O.N.); t.idrissova@sci.kz (T.I.); vzhu@mail.ru (V.Z.); slava.piscal@mail.ru (V.P.); zhakansadykov@gmail.com (Z.S.)

<sup>2</sup> Institute for Nuclear Research of the Russian Academy of Sciences, Moscow 117312, Russia; rauf\_m@mail.ru

<sup>3</sup> Skobeltsyn Institute of Nuclear Physics, Lomonosov Moscow State University, Moscow 119991, Russia; v\_i\_galkin@mail.ru

<sup>4</sup> Faculty of Physics and Technology, Al-Farabi Kazakh National University, Almaty 050040, Kazakhstan

<sup>5</sup> Tien-Shan High-Mountain Scientific Station of the Lebedev Physical Institute of the Russian Academy of Sciences in the Republic of Kazakhstan, Almaty 050020, Kazakhstan

<sup>6</sup> College of New Materials and Nanotechnologies, National University of Science and Technology "MISIS", Moscow 119071, Russia

\* Correspondence: aarginova7@gmail.com

**Abstract:** In high-altitude experiments to study the central cores of EAS at  $E_0 \gtrsim 10^{16}$  eV ( $\sqrt{s} \gtrsim 5$  TeV) using X-ray emulsion chambers and ionization calorimeters, phenomena such as the coplanarity of the arrival of the most energetic particles in super families of  $\gamma$ -rays and hadrons and a so-called Tien Shan effect (too slow absorption of cascades initiated by high-energy hadrons in the calorimeter) were observed. These effects could not be reproduced within the framework of theoretical models of the 80s and 90s. The coplanarity is explained via a process of coplanar generation of the most energetic secondary particles in interactions of super high-energy hadrons with nuclei of air atoms. Perhaps the Tien Shan effect could be explained using a high cross section for the generation of fragmentation-region charmed hadrons. To study these phenomena, a new set of detectors has been developed, including the world's highest high-mountain ionization calorimeter, "Hadron-55". This paper presents the initial experimental results.

**Keywords:** cosmic rays; ionization-neutron calorimeter; scintillation detector; ionization chambers; hadron cascade; extensive air shower (EAS); Monte Carlo simulation



**Citation:** Sadykov, T.; Mukhamedshin, R.; Galkin, V.; Argynova, A.; Almenova, A.; Argynova, K.; Makhmet, K.; Novolodskaya, O.; Idrissova, T.; Zhukov, V.; et al. First Results of Studying EAS Cores Using a High-Mountain Ionization Calorimeter. *Particles* **2024**, *7*, 40–51. <https://doi.org/10.3390/particles7010003>

Academic Editors: Francesco Maria Follega and Francesco Nozzoli

Received: 25 November 2023

Revised: 18 December 2023

Accepted: 20 December 2023

Published: 28 December 2023



**Copyright:** © 2023 by the authors. Licensee MDPI, Basel, Switzerland. This article is an open access article distributed under the terms and conditions of the Creative Commons Attribution (CC BY) license (<https://creativecommons.org/licenses/by/4.0/>).

## 1. Introduction

Modern experiments with cosmic rays use several models of the interaction of high- and ultra-high-energy hadrons with the nuclei of air atoms and the generation of secondary particles, as well as the development of the so-called extensive air showers (EASs) in the atmosphere. However, all these models cannot accurately reproduce the entire set of observed characteristics of EASs.

In the 1970s, when studying EASs at the high-mountain scientific station Tien Shan (3340 m a.s.l.), a slowdown in the absorption rate of high-energy hadron cascades ( $\gtrsim 10$  TeV) was observed in the so-called Big Ionization Calorimeter (BIC). The BIC had a lead absorber with the total thickness of  $850 \text{ g/cm}^2$  (about five mean free paths (m.f.p.s) for the interaction of protons in lead) [1–5]. It was found that the absorption length  $L(E_h)$  of the hadronic component in EAS cores in the BIC grows with increasing hadron energy  $E_h$ . It was shown after the discovery of charmed particles that this effect can be explained by assuming that in hadronic interactions the cross section for the production of such particles, which carry

away a significant fraction of the energy of the interacting hadrons, reaches ~30% of the inelastic proton–nucleus cross section [6].

An ionization calorimeter with a thickness of about six (or more) hadron interaction mean free paths could help study this very interesting effect.

In high-altitude XREC experiments, the Pamir (4300 m a.s.l.) [7–9] and Mt. Kanbala [10] collaborations observed a tendency for the most high-energy particles (and/or narrow electromagnetic subcascades) with energies  $E \gtrsim 10$  TeV to arrive coplanarly in so-called  $\gamma$ -ray–hadron superfamilies with energies  $\sum E_\gamma > 700$  TeV near the axes of relatively “young” EASs that have not reached the maximum of their development at the time of registration at the observational level. These showers are mainly initiated by protons and helium nuclei of primary cosmic radiation (PCR).

The overall picture is complemented by two  $\gamma$ -ray–hadron families with superhigh energies ( $\sum E_\gamma > 1$  PeV) and very high coplanarity of the most energetic particles detected using the emulsion technique at high altitudes in the stratosphere (where the characteristics of showers are much more sensitive to parameters of first interactions of PCR particles in the atmosphere). The experiments were carried out on board a balloon (*Strana* [11–13]) and a Concorde jet (*JF2af2* [14,15]).

The probability of obtaining the entire set of these experimental results is too small ( $\lesssim 10^{-10}$ ) [16–18] to explain this result via cascade fluctuations.

In general, we can conclude [16] that (1) this phenomenon is associated with the most energetic particles generated in interactions at the early stage of EAS development; (2) this process is not reproduced using models based on the quantum chromodynamics (QCDs) and quark-gluon string (QGS) models applied in high-energy cosmic ray physics; and (3) the cross section for coplanar particle generation (CPG) is relatively large.

Theoretical concepts relate the generation of coplanar particles to (1) the angular momentum of the quark-gluon string rotated by interacting hadrons [19]; (2) semihard double inelastic diffraction [20], accompanied by some stretching of the QGS inside the diffraction cluster between spectator quarks and one semihard scattered quark of the hadron interacting with the nucleus of an air atom; (3) leading systems with very high spin [21,22]; and (4) temporary evolution of a three-dimensional space into a two-dimensional one [23,24].

The hypotheses [19–22] imply that the coplanar plane is determined by large transverse momenta, while the momentum components directed perpendicular to this plane still have the traditional values inherent in modern models of hadronic interactions. The hypothesis [23,24] assumes the possibility of temporal evolution of the dimension of space from three to two dimensions at sufficiently high energies. As a result, this hypothesis does not require a significant change in the average values of the transverse momenta, but it postulates their localization in a certain plane.

The aforementioned experimental data observed in the EAS cores show that we do not yet understand all the features of hadronic interactions. Unfortunately, these phenomena cannot be studied in experiments carried out at the Large Hadron Collider (LHC). The specificity of the LHC design allows us to study in detail, mainly, only particles in the central kinematic region ( $|\eta, y| \lesssim 4\text{--}5$ ). However, it is possible to continue studying these phenomena in high-mountain experiments with cosmic rays.

The scale of coplanar events observed with XREC, which are characterized by very high lateral resolution ( $\sim 100$   $\mu\text{m}$ ), is small, mostly around 1 cm or less, which is consistent with selection of events caused by hadron interactions at altitudes of 1–2 km above the XREC detector. The ionization calorimeter at the altitude of the Tien Shan station has a much coarser lateral resolution, determined by the width of its ionization chambers (IC) ( $\sim 12$  cm). In this case, searching for showers with several of the most energetic subcores in the central region will lead to the selection of events created by hadron–nucleus interactions at much higher altitudes ( $\sim 10$  km) above the calorimeter, where the produced high-energy hadrons initiate subcascades arriving at the upper surface of the calorimeter.

A thick ionization calorimeter will make it possible to study the experimental results discussed above, namely, the too-slow ionization absorption and the coplanarity of the arrival of the most energetic subcores in the region of the EAS cores.

Note that in some works (see [25], e.g.), the authors associate non-standard phenomena observed in studies at Tien Shan High Mountain Scientific Station with EASs initiated by strangelets (particles of strange quark matter), which may also be present in the PCR [25].

## 2. Design of the “Hadron-55” Ionization-Neutron Calorimeter

### 2.1. Complex Installation “Hadron-M”

The complex installation “Hadron-M” is located at an altitude of 3340 m a.s.l. and includes an ionization-neutron calorimeter (INC) “Hadron-55” with an area of 55 m<sup>2</sup>, total absorber thickness of 1244 g/cm<sup>2</sup>, nine rows of ICs, and one row of neutron detectors, as well as two shower systems of scintillation detectors. The effective area of the “Hadron-M” installation is 30,000 m<sup>2</sup>. The “Hadron-55” is located in a laboratory building with an area of 324 m<sup>2</sup>. An external shower scintillation-detector (SD) system is located outside the building in concentric circles with radii of 25, 40, and 100 m, with four SDs in each circular zone. Several neutron counters included in the “Hadron-55” are installed to obtain information about the interactions of EAS hadrons in the INC absorber.

### 2.2. Design of the “Hadron-55”

The diagram of the calorimeter, consisting of an upper part (the so-called gamma block) and a lower part (the so-called hadron block) is shown in Figure 1 (Figure 4, [26]). The gamma block and the hadron block are separated vertically by 2.2 m for experiments related to the search for charmed particles.

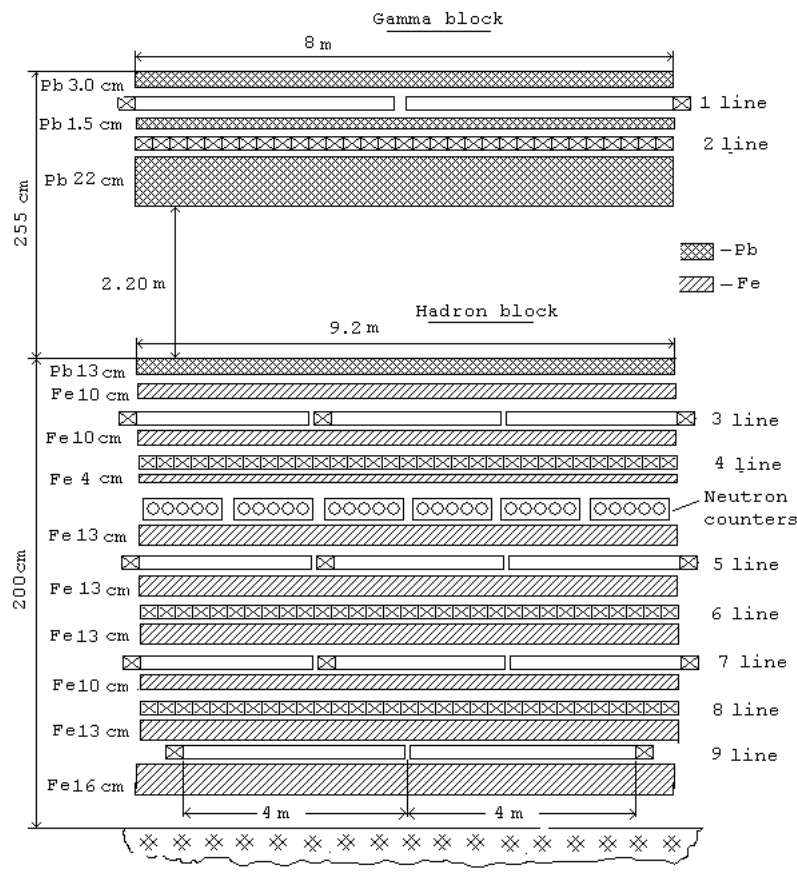
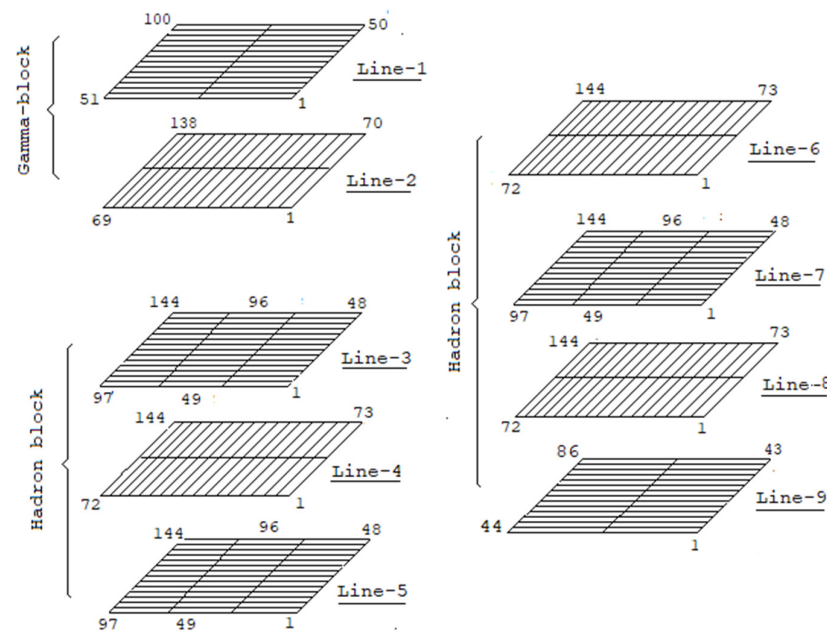


Figure 1. Cross section of the “Hadron-55” calorimeter.

The gamma block consists of two IC rows, namely, 100 chambers in the first row and 138 chambers in the second one, separated by lead, with a total thickness of 3 cm + 1.5 cm + 22 cm = 26.5 cm (310 g/cm<sup>2</sup>).

The hadron block consists mainly of the iron absorber with cavities in which ionization chambers are installed. First of all, this block is used to measure the energy released in the absorber material via the hadronic component arriving in the EAS cores. This makes it possible to study in more detail characteristics of the interactions of cosmic radiation particles and the mass composition of primary cosmic rays. The hadron block contains 7 IC rows (144 chambers in each row) located in a mutually perpendicular position with an iron absorber between the rows.

Figure 2 shows the layout of nine rows of ionization chambers of the gamma block and hadron block of the calorimeter. The X coordinate axis is directed across the even rows of chambers (rows 2, 4, 6, 8) and allows determination of the position of the shower core along the X axis with an accuracy of the chamber width (12 cm). The Y axis is directed across the ionization cameras of the odd rows (rows 1, 3, 5, 7) of cameras, which also makes it possible to determine the Y coordinates of the shower axis.



**Figure 2.** Layout of the rows of ionization chambers from the 1st to the 9th row of the gamma block and hadron block of the “Hadron-55”.

Characteristics of ionization chambers (IC):

- The lengths of the chambers are 400 cm (1st row) and 300 cm (rows 2–9).
- The IC width is 11.5 cm, and the height is 6 cm.
- The case material is copper block that is 2 mm thick.
- The chambers are filled with argon gas under a pressure of 4.5–5 atm.
- The central thread diameter is 3 mm.
- The total number of chambers is 1200 pieces.

### 2.3. Registration and Analysis of Experimental Data from “Hadron-M”

The database system of the complex installation “Hadron-M” operates under the control of the PostgreSQL server program, which can be accessed via a local network using remote client programs with specific requests for data processing. The database is available at [www.tien-shan.org](http://www.tien-shan.org) (accessed on 21 December 2023).

The experimental data bank of the “Hadron-M” installation has a two-level structure. The first-level bank (Bank-0) contains real experimental physical events, as well as test

events, in the form of recorded codes of pulse amplitudes of each detector, which are summed and converted into a binary ADC code. The test-event registration mode, used for operational control of the calorimeter, is intended to analyze the operation of individual channels of the registration system. The second-level bank (Bank-1) contains data that was initially recorded in physical mode in Bank-0, but which takes into account the calibration characteristics for each individual channel. In this case, the ADC codes are converted into ionization values, which, in turn, are converted into millivolts, which are proportional to the energy  $E_{cal}$  of the EAS hadron component released in the calorimeter.

The EAS power (number of charged particles,  $N_e$ ) is determined as the sum of particles in all chambers of the eight rows of the INC.

The number of particles  $N_{ij}$  in each  $i$ -th chamber of the  $j$ -th row is calculated as the result of dividing the amplitude of the signal at the output of the chamber amplifier,  $U_k$ , by the corresponding value of the standard signal from the passage of one charged particle,  $U_{oe}$ , i.e.,  $N_{ij} = U_k / U_{oe}$ .

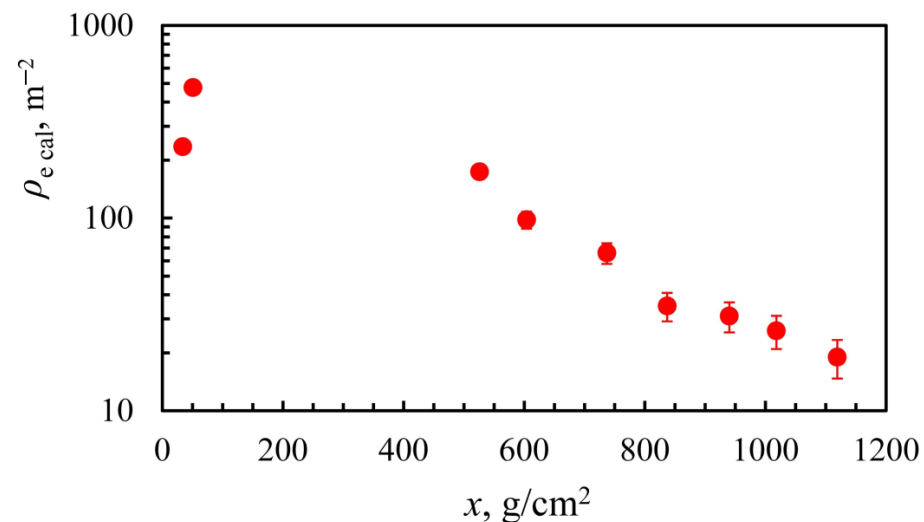
To determine the amplitude of the signal from a single particle,  $U_{oe}$ , a test bench is assembled, including an ionization chamber, an amplifier combined with an ADC (analog-to-digital converter), and a computer. The amplitude spectrum of pulses generated by single background cosmic-ray particles is recorded using this test bench.

The peak value of the spectrum is taken as the amplitude of the signal from one charged particle, namely,  $U_{oe} = 0.39$  mV/particle.

To take into account the variation of argon gas pressure in the ionization chambers (~10%) and channel gains (~20%), the calibration of registration channels is regularly performed at the installation. The calibration is stored in the computer memory for each channel  $N_{ij}$  and is taken into account when forming the database.

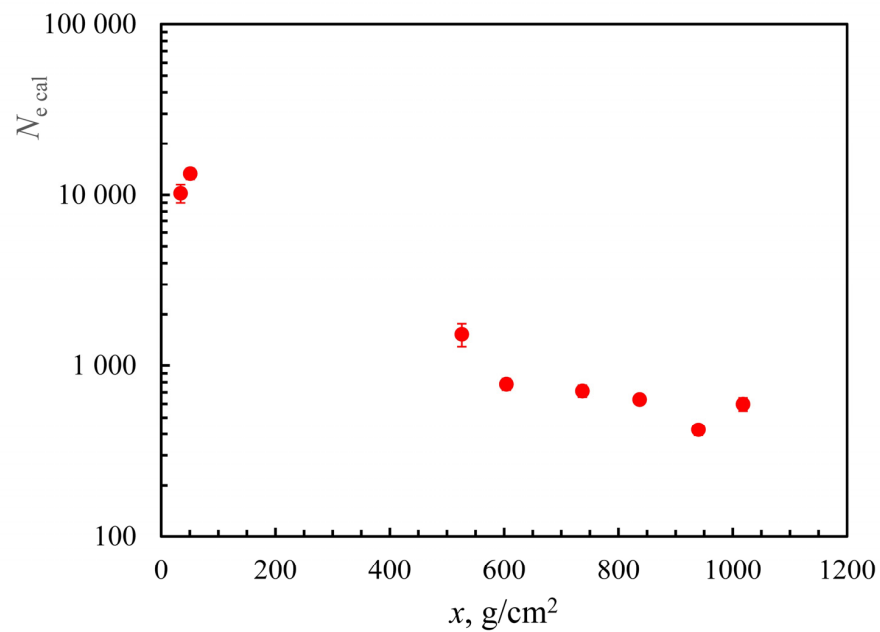
#### 2.4. Experimental Data from the “Hadron-55”

Figure 3 shows the dependence of the density of charged particles in the ionization chambers of the “Hadron-55”,  $\rho_{e\text{ cal}}, \text{ m}^{-2}$ , on the amount of matter of the absorber, averaged over all recorded showers, regardless of the location of the fall of the main EAS core.



**Figure 3.** Dependence of the density of charged particles in the ionization chambers,  $\rho_{e\text{ cal}}, \text{ m}^{-2}$ , on the amount of absorber matter ( $\text{g}/\text{cm}^2$ ), averaged over all registered EASs.

Figure 4 shows the dependence of the shower power (the number of registered charged particles in the ionization chambers) of the “Hadron-55” calorimeter,  $N_{e\text{ cal}}$ , on the amount of the absorber matter, averaged over a hundred showers, the main cores of which arrived on the surface of the calorimeter. The RMS errors shown in Figure 4 characterize only fluctuation deviations of the characteristics of individual showers from the average values.



**Figure 4.** Dependence of the number of charged particles registered by the “Adron-55” ICs,  $N_{e\text{ cal}}$ , on the amount of absorber matter ( $\text{g}/\text{cm}^2$ ) of the “Hadron-55” INC, averaged over showers, the cores of which arrived on the surface of the calorimeter.

Recall that the two leftmost points in Figures 3 and 4 refer to the gamma block, i.e., they characterize mainly the low-energy electron–positron and muon components. The remaining points on the graph are mainly determined by EAS hadrons, which interact directly in the absorber matter, producing particles, in particular neutral  $\pi^0$  mesons, which almost immediately decay into  $\gamma$ -rays, which initiate electron–photon cascades in the dense absorber matter.

It can be seen that although the spectra are naturally qualitatively similar to each other, there are also some differences. In particular, the rightmost point in Figure 4, corresponding to an absorber thickness of  $10^{18} \text{ g}/\text{cm}^2$ , is located noticeably higher than the previous point, which corresponds to a depth of  $940 \text{ g}/\text{cm}^2$ . Further research is needed to explain this experimental result, which, on the one hand, may have physical reasons (e.g., being similar to the Tien Shan effect [1]) and, on the other hand, can be explained using methodological reasons (e.g., edge effects).

In particular, a large-scale simulation of both the EAS development in the atmosphere and the processes of recording EAS particles in the “Hadron-55” calorimeter are absolutely necessary.

### 3. Simulation of EAS Development in the Atmosphere

#### 3.1. Simulation of Nucleus-Initiated EAS Development

A simulation of the development of EASs, initiated by protons and nuclei of primary cosmic radiation of ultra-high energies, and consisting of a huge number of hadrons, electrons, positrons,  $\gamma$ -rays, and muons at the observation level, was started. The simulation results using the standard CORSIKA7.7500 software package [27] were obtained in the form of observable EAS characteristics (type, momenta, time, and angles of arrival of each particle at the observation level).

When using the CORSIKA package, it is possible to choose from several models of interaction of hadrons with atom nuclei in the atmosphere. For our calculations, we used the QGSJET II-04 [28] model, based on the ideologies of quark-gluon strings and quantum chromodynamics, which explain the generation of hard hadron jets with significant transverse momenta. The model has demonstrated promising outcomes in measuring hadron production at accelerator energies [28–31].

The development of vertical EASs initiated by various primary cosmic nuclei (from protons to iron nuclei, Fe) with energies of 1, 10, 30, and 100 PeV was simulated, starting from the boundary of the atmosphere (112.83 km above sea level, CORSIKA standard) to the level of the “Hadron55” location. The following energy thresholds were used when simulating: 30 MeV for electrons/positrons and gamma-rays and 1 GeV for hadrons and muons. The lateral and energy characteristics of  $e^\pm$ ,  $\gamma$ ,  $\mu$ , and hadrons were obtained at various threshold values,  $E_{\text{thr}}$ .

### 3.2. Simulation of Strangelet-Initiated EAS Development

A simulation of the development of EAS initiated by so-called strangelets, i.e., hypothetical PCR particles of strange quark matter (SQM) [25], was also started. The main differences between strangelets and traditional nuclei are, firstly, the much larger contribution of strange quarks, and secondly, the much larger baryon number. SQM can be divided into three classes [25] depending on value of the baryon number  $A_s$ :

- (1) Block SQM:  $A_s > 10^7$ . In a large volume of SQM, the following equality holds for the ratio of the number of quarks:  $n_v = n_d = n_s$ , while its electric charge is zero.
- (2) Stable SQM particles (strangelets) ( $10^2 < A_s < 10^7$ ). The model estimate of the stability region of strangelets is  $A_s > 300\text{--}1000$ . In fact, such strangelets are quasi-nuclei with a lower density (compared to ordinary nuclei) and a positive electric charge  $Z = (0.03\text{--}0.1) A_s$ .
- (3) Unstable SQM particles:  $A_s < 100$ .

Theoretical uncertainties do not allow us to unambiguously select the class of SQM for EAS simulation.

Therefore, it is reasonable to start EAS simulation with stable strangelets, assuming that  $A_s = 2000$  and considering the strangelet as a very large quasi-nucleus, for which the interaction cross section in air is equal to  $\sigma_{s\text{-air}} \approx \sigma_{pp} (A_s^{2/3} + A_{\text{air}}^{2/3})$ .

Let the average path to the first interaction of a strangelet be  $\lambda_s^1 = 1 \text{ g/cm}^2$ . In this interaction, some of the baryons interact and leave the body of the strangelet, both individually and as ordinary nuclei.

With each interaction, free ordinary nuclei with mass  $A_i$  are formed. Moreover, the heavier the nucleus, the less likely it is to be born. In calculations, it is assumed that primary nuclei belong to one of the main groups. Therefore, in each of the strangelet interactions, one or several nuclei with masses  $A = 1$  (protons), 4 (He), 12 (C), 32 (S), or 56 (Fe) are born.

In reality, in each Poisson interaction, the number of breakaway nucleons  $N_{\text{nucl}}$  is sampled with an average number of breakaway nucleons  $\langle N_{\text{nucl}} \rangle = 12$ , which then form a nucleus or nuclei from the given set.

The interaction cross section for the remaining part of the strangelet at each subsequent  $k + 1$ -st interaction will be determined by the baryon number  $A_s^k$ . Naturally, for each  $k$ -th residue of the strangelet, the average ranges rank as  $\lambda_s^k > \dots > \lambda_s^2 > \lambda_s^1$ .

During the development of an EAS, more than a hundred interactions of the strangelet take place until it is completely disintegrated into individual protons, neutrons, and nuclei of various atomic weights, initiating independent subcores within the central core of an EAS. All resulting subcascades are traced to the observation level (3340 m a.s.l.) with thresholds of 30 MeV for electrons/positrons and gamma-rays and 1 GeV for muons and hadrons.

To simulate cascades from protons and nuclei produced during the breakup of strangelets and the observed characteristics of EASs, the standard CORSIKA package and the QGSJET II-04 model are used.

### 3.3. First Results of the Simulation of EAS Development

A simulation of vertical EASs initiated by protons, iron nuclei, and strangelets with energy  $E_0 = 100 \text{ PeV}$  was carried out.

Figure 5 shows the energy spectra of hadrons with energies  $E_h > 100 \text{ GeV}$  in these showers. It can be seen that the spectrum of hadrons in proton-initiated EASs is the flattest, and it even contains hadrons with energies  $E_h > 300 \text{ TeV}$ . Accordingly, the hadron spectrum

in the EAS initiated by strangelets is the softest. This is not surprising, since initially in strangelets with  $A_s = 2000$ , the energy per nucleon is only  $E_{\text{nucl}} = 50$  TeV. In fact, hadrons with maximum energy are nucleons of the primary strangelet that have passed through the atmosphere without a single interaction at the observational level.

10 × 100 PeV EAS, hadron energy spectra at 3340 m a.s.l.

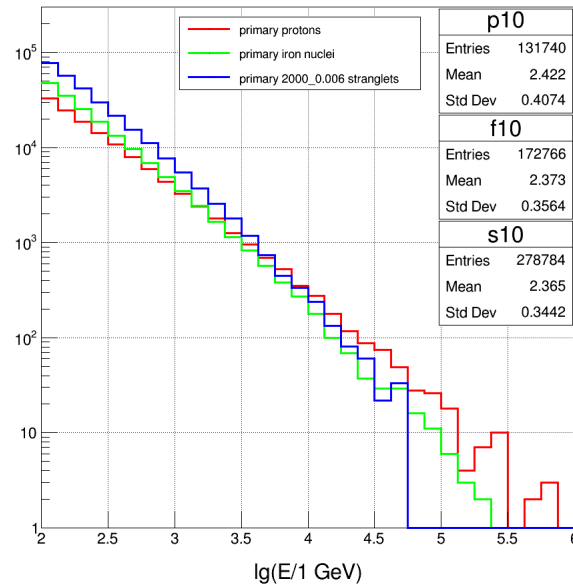


**Figure 5.** Energy spectra of hadrons with energy  $E_h > 100$  GeV in EASs initiated by PCR protons, iron nuclei, and strangelets with energy  $E_0 = 100$  PeV.

Figure 6 shows the dependence of the average hadron energy (at  $E_h > 100$  GeV) on the distance from the EAS axis in proton-, iron-, and strangelet-initiated showers with energy  $E_0 = 100$  PeV. It can be seen that the average energy of hadrons in proton-initiated showers is noticeably higher than in iron-initiated showers. The difference is even greater compared to showers from strangelets. However, this is to be expected based on the spectra presented in Figure 5.

10 × 100 PeV EAS, secondary hadrons,  $\langle E \rangle$  vs.  $r$

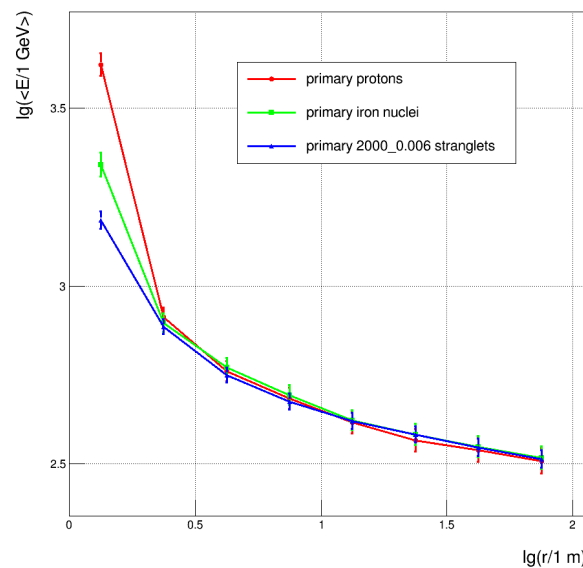


**Figure 6.** Dependence of the average energy of hadrons (at  $E_h > 100$  GeV) on the distance to the EAS axis in showers initiated by PCR protons, iron nuclei, and strangelets with energy  $E_0 = 100$  PeV.

Figure 7 shows the lateral distributions of hadrons (at  $E_h > 100$  GeV) in showers initiated by protons, iron nuclei, and PCR strangelets with energy  $E_0 = 100$  PeV. It can be seen that the distribution at large distances from the axis in proton EASs is approximately five times lower than the distribution in EASs from strangelets.

10 × 100 PeV EAS, hadron lateral distribution functions at 3340 m a.s.l.

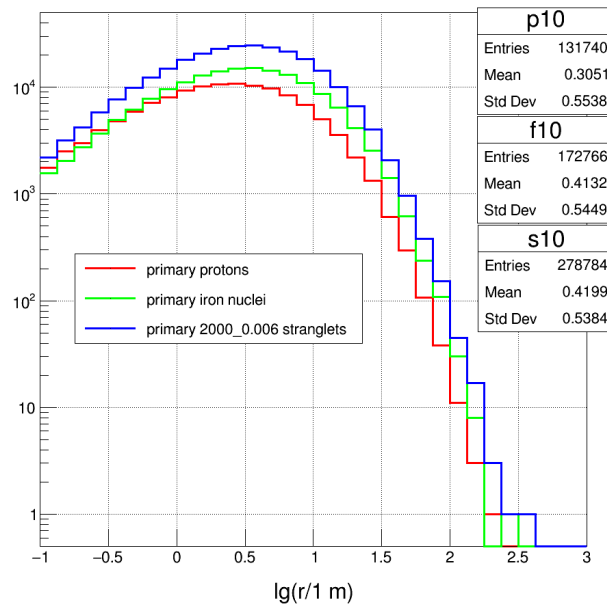


**Figure 7.** Lateral distribution of hadrons (at  $E_h > 100$  GeV) in showers initiated by PCR protons, iron nuclei, and strangelets with energy  $E_0 = 100$  PeV.

Similar distributions have been obtained for electrons/positrons and muons.

#### 4. Simulation of the “Hadron-55” Response to the Passage of EAS Particles

##### 4.1. Physical Foundations

To simulate the passage of EAS particles through the “Hadron-55” calorimeter, the Hadr55 program was developed based on the Geant4 package (versions 4.11.0 and 4.11.1.1) [28]. A three-dimensional model of the “Hadron-55” calorimeter and the characteristics of the materials of which it consists were entered into Geant4.

Electromagnetic interactions were simulated according to the physical list G4EmStandardPhysics\_opt3 [28].

Hadronic interactions were simulated using the FTFP\_BERT model, which is used in Geant4 by default and assumes the reproduction of elementary interactions using the Fritiof parton model and Bertini model of the intranuclear cascade [28].

##### 4.2. Geometry of the Mathematical Model “Hadron-55”

The geometry of the calorimeter was constructed based on its general appearance shown in Figures 1 and 2, as well as specific data on ionization chambers and absorber layers.

The densities of lead and iron are defined as 12.5 and 7.8 g/cm<sup>3</sup>, respectively. The IC structure is reproduced in accordance with the description: body material is copper with a density of 8.92 g/cm<sup>3</sup>, external dimensions are 400 cm × 11.5 cm × 6 cm for the first row and 300 cm × 11.5 cm × 6 cm for subsequent rows; and the IC wall thickness is 2 mm.

Currently, the response of neutron counters is not simulated and is approximated only via homogeneous polystyrene blocks 10 cm thick with a density of 1.032 g/cm<sup>3</sup>.

##### 4.3. The Saved Information

In Geant4, an event is considered to be the whole set of phenomena that occur after entering the detector of a single particle (hadron,  $\gamma$ -ray, muon, etc.). In our case, the event is considered to be the passage of some part of the EAS particles through the calorimeter,

and the total energy release of these particles in each of the ionization chambers is of interest. The final image of the shower in energy releases is saved in the text file `ioni_nch_*`, where `*` means the specification of the event (type and energy of the particle). The same file contains information about the number of charged particles entering each ionization chamber. The saved information can be changed and/or supplemented.

As an example, Figure 8 shows tracks from a single proton with energy of 5 GeV. It is challenging to depict all tracks of an EAS event in the calorimeter due to the multitude of tracks.

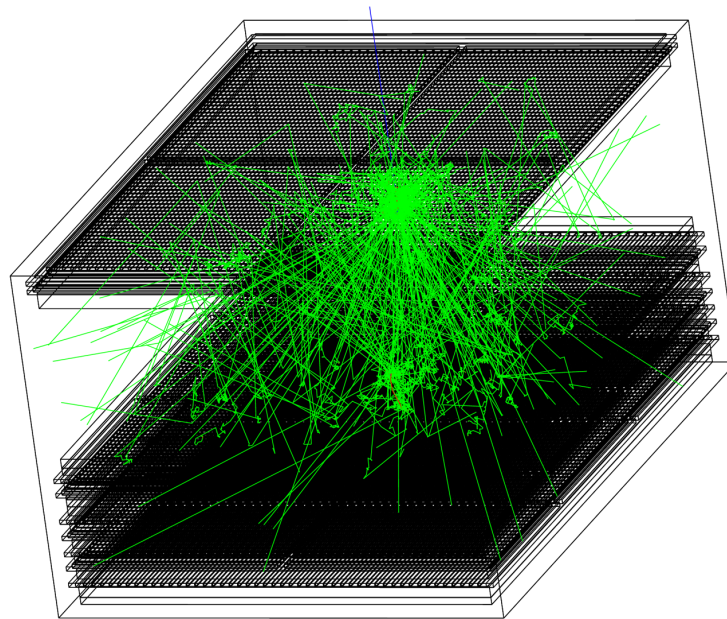


**Figure 8.** Image of tracks (in green) from a single proton with an energy of 5 GeV.

#### 4.4. Resources Required for Simulating Events in the Calorimeter

The simulation of the passage of EASs through the calorimeter takes place in two stages. In the first stage, where the cascade of particles in the air must be calculated and the particles that have reached the observation level recorded, CORSIKA is used. At the second stage, some of these particles that fall on the calorimeter are traced through the calorimeter structures using Hadr55.

The simulation of a particle cascade in the atmosphere from ultra-high-energy primary pulse particles places serious demands on the computers used: the simulating time for one event varies from ~3 min at energy  $E_0 = 1$  PeV to 3–4 h at  $E_0 = 100$  PeV. The volume of output binary files can reach several gigabytes per event (depending on the thresholds that are set).

Utilizing CORSIKA results for simulating calorimeter processes demands even more time. At the selected thresholds (30 MeV for electrons and  $\gamma$ -rays and 1 GeV for muons and hadrons), the number of traceable secondary particles for primary energies of 100 PeV can reach tens of millions. Tracking 10,000 secondary particles takes from 1 to 40 min with an average time of several minutes, and tracking tens of millions of particles takes a thousand times longer, i.e., a few days. Such a large spread is due to the wide energy spectrum of the incident particles: low-energy particles are quickly absorbed, and higher-energy particles cascade, requiring significant simulating time. As a result, tracking one EAS initiated by a particle of primary cosmic radiation with energy of 100 PeV takes 2–3 days on one nucleus. The disk space requirements in the tracking process are about 1 GB per event, if we select only the particles falling into the calorimeter from the CORSIKA output file and place them in a text file from which the Hadr55 code will read them. At the end of the calculation, only a small text file of about 50 kb remains.

Thus, the simulation of a large number of events in a calorimeter requires a separate server or servers capable of generating artificial events around the clock.

## 5. Conclusions

The first experimental results of studies of EAS cores were obtained at an altitude of 3340 m a.s.l. using the high-altitude ionization calorimeter “Hadron-55” with an area of 55 m<sup>2</sup> and a thickness of about six proton m.f.p.s for interaction.

In EASs, the cores of which arrive at the upper plane of the “Hadron-55”, the average intensity of hadrons at great depths is higher than for the totality of all showers. In the first case, there is a tendency to slow down the absorption of hadrons.

The simulation of EASs initiated by PCR protons, iron nuclei, and hypothetical strangelets of primary cosmic rays and simulation of processes of the passage of EAS cores through the “Hadron-55” calorimeter have begun.

Experimental and simulated results are very preliminary.

**Author Contributions:** Conceptualization and methodology, T.S., R.M. and V.G.; Software and visualization, V.G., K.A. and Z.S.; Resources and data curation, V.P., K.M., O.N., A.A. (Alia Argynova) and A.A. (Aidana Almenova); Writing—review and editing, R.M. and A.A. (Aidana Almenova); Writing—original draft preparation, R.M. and V.G.; Project administration and funding acquisition, T.S., T.I. and V.Z. All authors have read and agreed to the published version of the manuscript.

**Funding:** This research is funded by the Science Committee of the Ministry of Science and Higher Education of the Republic of Kazakhstan (Grant No. AP19679396).

**Data Availability Statement:** The experimental data from “Hadron-M” can be found in [www.tien-shan.org](http://www.tien-shan.org) accessed on 19 December 2023.

**Conflicts of Interest:** The authors declare no conflict of interest.

## References

1. Amineva, T.P.; Glavach, T.G.; Aseikin, V.S.; Vavilov, Y.N. Installation for studying extensive air showers and nuclear interactions of cosmic-radiation particles with an energy of 1012–1016 eV. *Trudy FIAN* **1970**, *46*, 157. (In Russian)
2. Aseikin, V.S.; Bobova, V.P.; Goryacheva, G.Y.; Nikolsky, S.I.; Yakovlev, V.I. Absorption of the energy flux in the cores of extensive air showers. *Izv. AN USSR* **1974**, *38*, 998–1002. (In Russian)
3. Yakovlev, V.I. Long flying component: Recent data and interpretation. *AIP Conf. Proc.* **1993**, *276*, 154.
4. Nikolsky, S.I.; Yakovlev, V.I.; Pavljuchenko, V.P. Hadronic Cascades with Anomalous Absorption in the Lead. In Proceedings of the 15-th International Cosmic Ray Conference, Plovdiv, Bulgaria, 13–26 August 1977; Volume 8, p. 130.
5. Nikolskaya, N.M.; Pavlyuchenko, V.P.; Yakovlev, V.I. *Parameters of High Energy Cores of EAS Detected with the Large Ionization Calorimeter on Tien Shan Mountain Station*; P.N. Lebedev Physical Institute: Moscow, Russia, 1989. (In Russian)
6. Dremin, I.M.; Madigozhin, D.T.; Yakovlev, V.I. Monte Carlo simulations of long-flying cascades in cosmic rays and leading charm at SSC. *AIP Conf. Proc.* **1993**, *276*, 534.
7. Bayburina, S.G.; Borisov, A.S.; Cherdyntseva, K.V.; Guseva, Z.M.; Denisova, V.G.; Dunaevskii, A.M.; Kanevskaya, E.A.; Maksimenko, V.M.; Pashkov, S.V.; Shaulov, S.B.; et al. Investigation of nuclear interactions in the energy range 10<sup>14</sup>–10<sup>17</sup> eV by the method of X-ray emulsion chambers in cosmic rays (Pamir experiment). *Trudy FIAN* **1984**, *154*, 3–141. (In Russian)
8. Kopenkin, V.V.; Managadze, A.K.; Rakobolskaya, I.V.; Roganova, T.M. Alignment in gamma-hadron families of cosmic rays. *Phys. Rev. D* **1995**, *52*, 2766–2774. [[CrossRef](#)] [[PubMed](#)]
9. Borisov, A.S.; Mukhamedshin, R.A.; Puchkov, V.S.; Slavatskiy, S.A.; Zdanov, G.B. On the nature of gamma-hadron family alignment. *Nucl. Phys. B (Proc. Suppl.)* **2001**, *97*, 118–121. [[CrossRef](#)]
10. Xue, L.; Dai, Z.Q.; Li, J.Y. Study on alignment of high energy -hadron family events with iron emulsion chambers. In Proceedings of the 26th International Cosmic Ray Conference, Salt Lake City, UT, USA, 17–25 August 1999; Volume 1, pp. 127–130.
11. Managadze, A.K.; Osedlo, V.I.; Roganova, T.M.; Sveshnikova, L.G.; Galkin, V.I.; Rakobolskaya, I.V.; Goncharova, L.A.; Kotelnikov, K.A.; Polukhina, N.G. Large transverse momenta in nuclear interaction at E<sub>0</sub> > 10<sup>16</sup> eV detected in stratosphere. *Phys. At. Nucl.* **2007**, *70*, 184–190. [[CrossRef](#)]
12. Apanasenko, A.V.; Dobrotin, N.A.; Goncharova, L.A.; Kotelnikov, K.A. Stratospheric superfamily with ΣE ~ 2 · 10<sup>15</sup> eV. In Proceedings of the 15th International Cosmic Ray Conference, Plovdiv, Bulgaria, 13–26 August 1977; Volume 7, pp. 220–225.
13. Osedlo, V.I.; Rakobolskaya, I.V.; Galkin, V.I.; Managadze, A.K.; Sveshnikova, L.G.; Goncharova, L.A.; Kotelnikov, K.A.; Martynov, A.G.; Polukhina, N.G. A superfamily with SE > 1015 eV observed in stratosphere. In Proceedings of the 27th International Cosmic Ray Conference, Hamburg, Germany, 8–15 August 2001; Volume 4, pp. 1426–1429.
14. Capdevielle, J.N. Analysis of one cosmic-ray collision near 10<sup>7</sup> GeV. *J. Phys. G Nucl. Phys.* **1988**, *14*, 503. [[CrossRef](#)]

15. Capdevielle, J.N.; Attallah, R.; Talai, M.C. Coplanar emission in gamma ray families, geometrical and dynamical coincidence or new mechanism? In Proceedings of the 27th International Cosmic Ray Conference, Hamburg, Germany, 8–15 August 2001; Volume 1, pp. 1410–1413.
16. Mukhamedshin, R.A. On coplanarity of most energetic cores in gamma-ray-hadron families and hadron interactions at  $\sqrt{s} > 4$  TeV. *J. High Energy Phys.* **2005**, *5*, 49. [[CrossRef](#)]
17. Mukhamedshin, R.A. Simulation of coplanar particle generation in hadron interactions at superhigh energies by the new FANSY code. *Nucl. Phys. B (Proc. Suppl.)* **2009**, *196*, 98. [[CrossRef](#)]
18. Mukhamedshin, R.A. FANSY 1.0: A phenomenological model for simulation of coplanar particle generation in superhigh-energy hadron interactions. *Eur. Phys. J. C* **2009**, *60*, 345–358. [[CrossRef](#)]
19. Wibig, T. Alignment in hadronic interactions. *arXiv* **2000**, arXiv:0003230.
20. Royzen, I.I. Theoretical approach to alignment phenomenon. *Mod. Phys. Lett. A* **1994**, *9*, 3517–3522. [[CrossRef](#)]
21. Yuldashbaev, T.S.; Nuritdinov, K.; Chudakov, V.M. Unusual family characteristics at energies above 10 PeV. *Nuovo Cim.* **2001**, *24*, 569–572.
22. Mukhamedshin, R.A. On a mechanism of coplanar generation of particles at superhigh energies. *Nucl. Phys. B (Proc. Suppl.)* **1999**, *75*, 141–144. [[CrossRef](#)]
23. Anchordoqui, L.A.; Dai, D.C.; Goldberg, H.; Landsberg, G.; Shaughnessy, G.; Stojkovic, D.; Weiler, T.J. Searching for the Layered Structure of Space at the LHC. *Phys. Rev. D* **2011**, *83*, 114046. [[CrossRef](#)]
24. Stojkovic, D. Vanishing Dimensions: A Review. *Mod. Phys. Lett. A* **2013**, *28*, 1330034. [[CrossRef](#)]
25. Shaulov, S.B.; Beyl, P.F.; Beysembaev, R.U.; Beysembaeva, E.A.; Bezshapov, S.P.; Borisov, A.S.; Cherdyntceva, K.V.; Chernyavsky, M.M.; Chubenko, A.P.; Dalkarov, O.D.; et al. Investigation of EAS cores. *EPJ Web Conf.* **2017**, *145*, 17001. [[CrossRef](#)]
26. Mukhamedshin, R.; Sadykov, T.; Serikkanov, A.; Aargynova, A.; Iskakov, B.; Argynova, K.; Mahmet, H.; Novolodskaya, O.; Idrissova, T.; Zhukov, V.; et al. Studies of Anomalous Phenomena in the Development of Electron-Nuclear Cascades in the EAS Cores Registered by a Modernized Complex Installation at Mountain Altitudes. *Appl. Sci.* **2023**, *13*, 2507. [[CrossRef](#)]
27. Heck, D.; Knapp, J.; Capdevielle, J.N.; Schatz, G.; Thouw, T. Report FZKA 6019. Forschungszentrum Karlsruhe. 1998. Available online: <https://www.iap.kit.edu/corsika/70.php> (accessed on 5 December 2023).
28. Allison, J.; Amako, K.; Apostolakis, H.; Araujo, H.; Arce Dubois, P.; Asai, M.; Barrand, G.; Capra, R.; Chauvie, S.; Chytracsek, R.; et al. Geant4 developments and applications. *IEEE Trans. Nucl. Sci.* **2006**, *53*, 270–278. [[CrossRef](#)]
29. Ostapchenko, S.S. Monte Carlo treatment of hadronic interactions in enhanced Pomeron scheme: QGSJET-II model. *Phys. Rev. D* **2011**, *83*, 014018. [[CrossRef](#)]
30. Ajaz, M.; Ismail, A.K.H.; Alrebdi, H.I.; Abdel-Aty, A.-H.; Ullah Mian, M.; Khan, M.A.; Waqas, M.; Khubrani, A.M.; Wei, H.-R.; AbdelKader, A. Simulation Studies of Track-Based Analysis of Charged Particles in Symmetric Hadron–Hadron Collisions at 7 TeV. *Symmetry* **2023**, *15*, 618. [[CrossRef](#)]
31. Ajaz, M.; Ashraf, M.U.; Waqas, M.; Yasin, Z.; Khubrani, A.M.; Hassan, S.; Ismail, A.H.; Li, L.L. Model studies of  $V^0$  production ratios in pp collisions at  $\sqrt{s} = 0.2, 0.9$  and 7 TeV. *Eur. Phys. J. Plus* **2023**, *138*, 14. [[CrossRef](#)]

**Disclaimer/Publisher’s Note:** The statements, opinions and data contained in all publications are solely those of the individual author(s) and contributor(s) and not of MDPI and/or the editor(s). MDPI and/or the editor(s) disclaim responsibility for any injury to people or property resulting from any ideas, methods, instructions or products referred to in the content.